Hydrological control of large hurricane-induced lahars: evidences from rainfall, seismic and video monitoring

Capra L.[1], Coviello V.[1], Borselli L.[2], Márquez-Hernández V.[1], Arámbula-Mendoza R.[3]

[1] *Centro de Geociencias, Universidad Nacional Autónoma de México (UNAM), Campus Juriquilla, Queretaro, México*

[2] *Instituto de Geología, Universidad Autónoma de San Luis Potosí, San Luis Potosí, México*

[3] *Centro Universitario de Estudios e Investigaciones en Vulcanología (CUEIV), Universidad de Colima, Colima, México.*

Abstract

The Volcán de Colima, one of the most active volcanoes in Mexico, is commonly affected by tropical rains related to hurricanes that form over the Pacific Ocean. In 2001, 2013 and 2016 hurricanes Jova, Manuel and Patricia, respectively, promoted tropical storms that accumulated up to 400 mm of rain in 36 hrs, with maximum intensities of 50 mm/hrs. Effects were devastating, with lahars activity along La Lumbre and Montegrande ravines, the most active channels on the S-SW flank of the volcano, lasting for several hours. Deep erosion along the river channels and several landslides at their side were observed, and damages to bridges and paved roads for the arrival of block-rich fronts resulted in the distal reach of the ravines. Based on data from real-time monitoring (including images, seismic records and rainfall data), the temporal sequence of these events is reconstructed and analyzed with respect to the rainfall characteristics and the hydrological response of the watersheds based on rainfall/infiltration numerical simulation. For the studied events, lahars occurred after 5-6 hours since rainfall started, lasted several hours and were characterized

by several pulses with block-rich fronts and a maximum flow discharge of 900 m^3/s. Rainfall/infiltration simulations were performer with the Flo-2D code using the SCS-Curve number infiltration model. Results show different behaviors for the arrival times of the first lahar pulses that correlate with the catchment's peak discharge for La Lumbre ravine and with the peaks in rainfall intensity for Montegrande ravine. This different behavior is strictly related to the area and shape of these two watersheds. Nerveless, for all the analyzed cases, the largest lahar pulse always corresponds with the last one and correlates with the maximum peak discharge of these catchments. Data here presented show that main pulses within a lahar are not randomly distributed in time, and they can be correlated with rainfall peak intensity and/or watershed discharge, depending on the watershed area and shape. This outcome has important implications for hazard assessment during extreme hydro-meteorological events since it could help in real-time alert. A stormwater was here designed based on the rainfall time distribution of hurricanes Manuel and Patricia and, in case on available weather forecasts, it can be used to run simulations prior to the event, and have an estimation of the time arrivals of main pulses, usually characterized by block-rich fronts that are responsible of damage to infrastructures and loss of goods and lives.

***Keywords**: lahar, hurricane, rainfall/infiltration simulation, Volcán de Colima, Mexico.*

1. Introduction

In past recent years hurricanes have had catastrophic effects on volcanoes of the world triggering lahars (sediment-water gravity-driven flows on volcanoes). One of the most recent episode is represented by the 2009 Hurricane Ida in El Salvador that caused

several landslides and debris flows from the Chichontepec volcano, killing 124 people, or by the 1998 Hurricane Mitch that triggered the collapse of a small portion of the inactive Casita volcano, originating a landslide that suddenly transformed into a lahar that devastated several towns and killed 2000 people (Van Wyk Vries et al., 2000; Scott et al., 2005). A similar event was observed in 2005 when tropical storm Stan triggered landslides and debris flows from the Toliman Volcano (Guatemala), causing more than 400 fatalities at Panabaj community (Sheridan et al., 2007). Other examples can be found at the volcanoes Pinatubo (Philippines), Merapi and Semeru (Indonesia), Soufriére (Montserrat), and Mt. Ruapehu (New Zealand), where tropical storms and heavy rainfall seasons have triggered high-frequency lahar events (Umbal and Rodolfo, 1996; Cronin et al., 1997; Lavigne et al., 2000; Lavigne and Thouret, 2002; Barclay et al., 2007; Dumaisnil et al., 2010; Doyle et al., 2010, de Bélizal et al., 2013).

Volcán de Colima (19°31'N, 103°37' W, 3860 m a.s.l., Fig. 1), one of the most active volcanoes in Mexico, is periodically exposed to intense seasonal rainfalls that are responsible for the occurrence of lahars from June to late October (Davila et al., 2007; Capra et al., 2010). Rain-triggered lahars represent a very common process during the rainy season (June-October) at Volcán de Colima (Davila et al., 2007; Capra et al., 2010; Vazquez et al., 2016a). They usually affect areas as much as 15 km from the summit of the volcano, with resulting damage to bridges and electric power towers (Capra et al., 2010), and are more frequent just after eruptive episodes such as dome collapse emplacing block-and-ash flow deposits (Davila et al., 2007; Vázquez et al., 2016b). Several hurricanes commonly hit the Pacific Coast each year and proceed inland as tropical rainstorm reaching the Volcán de Colima area. In particular, on 2011, 2013 and 2015 Jova, Manuel and

draining the edifice

Patricia ~~hurricane~~ respectively triggered long-lasting lahars along main ravines, causing ~~several~~ severe damages ~~on~~ to roads and bridges, ~~leaven uncommunicated for few days several~~ and leaving communities in a radius of 15 km from the volcano, cut off for several days.

Previous work (Davila et al., 2007; Capra et al., 2010) analyzed ~~the~~ lahars frequency at Volcán de Colima in relation ~~with the~~ to eruptive activity and ~~the~~ characteristics ~~of~~ rainfall ~~rainfalls~~. Lahars are more frequent at the beginning of the rainy season, during short (< 1 hour) stationary rainfall events with variable rainfall intensities and with only 10 mm of accumulated rainfall. This behavior has been attributed to a hydrophobic effect of soils on the volcano slope (Capra et al., 2010). In contrast, in the late rainy season, when tropical rainstorms are common, lahars are triggered depending on the 3-day antecedent rainfall and with intensities that increase as the total rainfall amount increases (Capra et al., 2010). The lahars record used for these previous studies was only based on seismic data. Since 2011 a visual monitoring system ~~have~~ has been installed on the Montegrande and La Lumbre ravines (Figure 1), based on which a quantitative characterization of some events (i.e. type of flow, velocity, flow discharge, flow fluctuation) have been possible (i.e. Vázquez et al., 2016a; Coviello et al., under revision). The aim of the present paper is to better understand ~~the~~ lahars initiation processes and their dynamical behavior, especially during hurricane events, when more damages ~~have~~ has been observed on inhabited area. In particular, the arrival time of the main lahar's front/surge at the monitoring stations is here analyzed with respect to ~~the~~ rainfall characteristics (rain accumulation and intensity) and in relation ~~with~~ to the hydrological response ~~of the watersheds~~ of watersheds based on a rainfall/infiltration numerical simulation. The occurrence of discrete surges within lahars ~~have~~ has been attributed to spatially and temporally distributed lahar sources, temporary damming, progressive entrainment of bed material or

change in slope angle (i.e. Iverson 1997; Marchi et al. 2002; Takahashi 2007; Zanuttigh and Lamberti 2007; Doyle et al., 2010; Kean et al., 2013). Without excluding previous models, data here presented shows that main pulses within a lahar are not randomly distributed in time, and they can be correlated with rainfall peak intensity and/or watershed discharge, depending on the watershed shape and hydrophobic behavior subject to the antecedent soil moisture. The lahars triggered by the hurricanes Jova, Manuel and Patricia are here used as they correspond with the best documented events occurred during past years, and they will be also compared with an extraordinary hydrometeorological event occurred at the begin of the rain season (11 June, 2013) to better show the drastic change on lahar initiation due to the hydrophobic effect of soils at Volcán de Colima. Based on rainfall distribution over time for the analyzed events, a stormwater is here designed, which can be used to run simulations prior to an event to have an estimation of the time arrivals of main pulses when weather forecast is available. The data here presented have important implication for hazard assessment during extreme hydrometeorological events as a complementary tool of an early warning system.

2. Methods and data

2.1. La Lumbre and Montegrande watersheds

The source area of lahars at Volcán de Colima corresponds to the uppermost unvegetated portion of the cone (Fig. 1 and 2a), with slopes between 35° and 20°, that also corresponds with an area of high connectivity, being prone to rills formation and erosive processes (Ortiz et al., 2017). The channels along main ravines have slopes from 15° up to 4° in the

more distal reach, they are flanked by densely vegetated terraces, up to 15 m high in average, that consist of debris avalanche and pyroclastic deposits from past eruptions (Figs. 2b and c) (Cortes et al., 2010; Roverato et al., 2011). Seven major watersheds ~~from 2 to 14 km^2~~ feed the main ravines draining from the volcano on the southern side (Fig. 1). La Lumbre is the largest watershed, with a total area of 14 km^2, and Montegrande is ~~in average with~~ the other catchments, with an area of 2 km^2 (Fig. 1). Beside the difference in total area, the Montegrande and La Lumbre watersheds are quite different in geometry. Montegrande catchment is elongated, with a maximum width of 800 m, 300 m ~~in~~ average. In contrast, the proximal portion of the La Lumbre catchment includes all the NW slope of the cone, ~~to then extent to a more elongated shape~~ towards SW, being up to 1500 m in width. These differences in area and shape can be correlated with a different response ~~in~~ water discharge ~~under~~ a rainfall event. In circular drainages, ~~as~~ the proximal portion of the La Lumbre watershed, all points are ~~quite~~ equidistant from the main river so all the precipitation reaches the river at the same time, concentrating a large volume of water. In contrast, in a more elongate basin, lateral drainages quickly drain water ~~on~~ the main channel at different points but with a lower total discharge. The Gravelius's index Kg (Bendjoudi and Hubert 2002), which is defined as the relation between the perimeter of the watershed (P) and that of a circle having a surface equal to that of a watershed (A):

$$Kg = \frac{P}{2\sqrt{\pi A}}$$

is here estimated for Montegrande watershed and for the upper, circular portion of La Lumbre watershed, obtaining values of 1.7 and 1.1 respectively. The lower the value, the more regular the basin's perimeter and the more prone it is to present high runoff peaks.

Based on these considerations, at La Lumbre watershed a larger volume of water concentrates along the main channel because of its larger surface and circular shape, but after a larger period of time respect to Montegrande ravine, where a minor volume of water quickly reaches the main drainage.

2.2 Lahar Monitoring at Volcán de Colima

In 2007, a monitoring program was implemented at Volcán de Colima. At the beginning, two rain gauges where installed to study lahar initiation (AR and PH sites, Figure 1) and lahar propagation was detected by the broadband seismic stations of RESCO, the seismological network of Colima University (Davila et al., 2007; Zobin et al., 2009; Capra et al., 2010). Afterwards, two monitoring station specifically designed for studying lahar activity were installed, in 2011 at the Montegrande ravine and in 2014 at La Lumbre ravine (MSMg and MSL respectively, Figure 1). Both stations consist of a 12 m-high tower with a directional antenna transmitting data in real time to RESCO facilities, a camcorder recording images each 2-4 secs with a 704 x 480 pixels in resolution, a rain gauge coupled with a soil moisture sensor, and a 10 Hz geophone (Vázquez et al., 2016a; Coviello et al., under revision). The rain gauge (HOBO RG3) records rain accumulation at one-minute intervals. At Montegrande ravine seismic data are also obtained from a 3 component Guralp CMG-6TD broadband seismometer installed at 500 m upstream from the monitoring site, sampling at 100 Hz (BB-RESCO, Figure 1).

Montegrande station detected lahars occurred during 2011 Jova and 2013 Manuel events, and lahars triggered during the 2015 Hurrican Patricia were only recorded by La Lumbre

159 station (Table 1). In fact, in 2011 only MgMS site was operating (as the BB-RESCO
160 station), and recorded the seismic signal of the lahar associated to Jova and Manuel. No
161 images are available since both events occurred during the night. The LMS station starts to
162 operate at the end of 2013 and was able to record the lahars associated to Hurricane Patricia
163 along the La Lumbre ravine (images and geophone data). In contrast, in 2015 the MgMS
164 was destroyed by pyroclastic flows during the 10-11 explosive activity, and in October
165 2015 the new station was still under construction. Only few pictures were acquired and they
166 are of low quality because of the abundant steam coming from the hot lahars since they
167 originated from the remobilization of fresh pyroclastic flow deposits (Capra et al., 2016).
168 The 11 June 2013 event was perfectly captured by the camera installed at the MgMS site
169 and the BB-RESCO recorded its seismic signal.

170 The seismic signal is here analyzed to detect the arrival of main flow fronts and discharge
171 variation. For this, only the amplitude of the signal is considered, which can be correlated
172 with the variation in the maximum peak flow discharge (Doyle et al., 2010; Vázquez et al.,
173 2016a). The seismic record is here compared with the available images to identify the main
174 changes in dynamic of the detected lahars. All the lahars here analyzed correspond to multi-
175 pulses events as classified by Vazquez et al. (2016a); they consist of long lasting lahars
176 presenting several pulses, each one characterized by a block-rich front followed by the main
177 body and dilute tail showing continuous changes in flow discharges. A detailed seismic
178 description of these types of lahars is available in Vázquez et al. (2016a), here we focus on
179 the number of main flow peaks and their arrival times (Table 2).

180

2.3. The hydrometeorological events

Hurricane Jova formed over the Pacific Ocean, hit the Pacific coast on October 12, 2011, as a category 2, and traveled inland toward Volcán de Colima. The hurricane arrived as a tropical storm at the town of Coquimatlán, just 10 km SW of the city of Colima with winds up to 140 km/h, and 240 mm of rain over 24 h (Fig. 3a). Severe damage was registered in inhabited area, including the city of Colima where floods damaged roads, bridges and buildings.

~~The 2013~~ Hurricane Manuel ~~of~~ (category 1), hit the pacific coast ~~during national holidays~~ (~~Fiestas Patria~~) causing several damage to mountainous region in Guerrero state, triggering several landslides that caused up to 96 deaths and left several villages ~~uncommunicated~~ as thousands of tourists ~~trapped~~ at Acapulco and Ixtapa international airports. At Volcán the Colima ~~rains~~ started on September 15 and lasted for more than 30 hrs with more than 300 mm ~~of accumulated rains~~ (Fig. 3a).

~~The 2015~~ Hurricane Patricia was considered as the strongest hurricane on record to affect Mexico. The system ~~starts~~ to develop on 18 October over the Pacific Ocean, strengthened into a hurricane shortly after 00:00 GMT 22 October and early on 23 October it reached its maximum category of 5. ~~But late on the same day, the system rapidly lost its strength.~~ It ~~landfalls~~ around 23:00 GMT along the coast of the Mexican state of Jalisco near Playa Cuixmala, about 60 km west-northwest of Manzanillo. ~~On the morning of the 23 October,~~ 2015 it continued to rapidly ~~weaken~~ as it ~~moves~~ on the Sierra Madre Occidental ~~high~~ ~~relieves~~. At Colima town, up to 400 mm of ~~rains~~ accumulated along 30 hours since the morning of 23 October (Fig. 3a). Lahars along the Montegrande ravine were hot since they

203 originated from the erosion of pyroclastic flow deposits emplaced during the 10-11 July
204 2015 eruption. Sever damages affected the Colima town and the volcano surrounding. A
205 bridge along the interstate was destroyed leaving uncommunicated La Becerrara village and
206 interrupting the traffic between Colima and Jalisco states.
207 Patricia and Manuel rainfalls show a similar behavior, with a progressive rain accumulation
208 along 28-30 hrs; in contrast, during Hurricane Jova, 200 mm of rain accumulated in less
209 than 15 hrs reaching a total of 240 mm during the following 13 hrs (Fig. 3a). These
210 differences are more evident plotting the 10-min accumulated value normalized over the
211 total accumulated rainfall (Fig. 3b). Average rainfall intensities calculated over a 10-min
212 interval range from 32 mm/hrs to 37 mm/hrs for Manuel and Patricia events respectively
213 and up to 43 mm /hrs for the Hurricane Jova (Table 2). Finally rainfall values were
214 calculated at selected intervals (15 m, 30 m, 45 mm, 1, 3, 6, 12, 18, 24, 28 hr) to design
215 possible storm rainfall distributions based on tropical rains associated to hurricanes
216 recorded so far at Colima Volcano (Table 2). Considering the similar behavior of the
217 Manuel and Patricia rainfalls, a stormwater can be designed considering their average
218 values (Fig. 3c) (i.e. NRCS, 2008), based on which a forecast analysis can be performed, as
219 will be discussed below.

220

221 **2.4. Rainfall simulations**

222 To better understand the lahar behavior and duration during extreme hydrometeorological
223 event at Volcán de Colima, rainfall simulations were performed with Flo-2D code (O´Brian
224 et al., 1993). The Flo-2D code routes the overland flow as discretized shallow sheet flow

using the Green-Ampt or the SCS Curve number (or combined) infiltration models. For the present work the SCS Curve Number (SCS-CN, i.e. Mishra and Singh, 2003) was selected. With this model, the volume of water runoff produced for the simulated precipitation is estimated through a single parameter that summarizes the influence of both the superficial aspects and deep soil, including the saturated hydraulic conductivity, type of land use, and humidity before the precipitation event. A similar approach was already used for modeling debris flow initiation mechanisms (i.e. Gentile et al., 2006; Llanes et al., 2015). To apply the SCS-CN model, it is necessary to classify the soil in one of four groups, each identifying a different potential runoff generation (A, B, C, D; USDA-NRCS 2007). The watershed of La Lumbre and Montegrande ravines were subdivided in two main zone: the unvegetated upper cone, and the main channel that consist of unconsolidated pyroclastic material with large boulders imbedded in sandy to silty matrix, and the vegetated lateral terraces. Lateral terraces consist of old pyroclastic sequences, with incipient soils and vegetated with pine trees and sparse brushes, with soils that show a hydrophobic behavior at the beginning of the rain season (Capra et al., 2010). In-situ infiltration tests were also performed based on which values of saturated conductivity were obtained in the range of 50 mm/h (nude soil) to 100 mm/h (vegetated) (Ortiz, 2017). Based on these observations, soils were classified between group A and B (Bartolini and Borselli, 2009). Curve Numbers for the vegetated terraces and for the nude soils were estimated in 75 and 80 respectively (in wet season, Hawkins et al., 1985; Ferrer-Julia et al. 2003). To perform simulation with the FLO-2D code, two polygons were traced to delimit the un-vegetated portion of the cone from the vegetated area of the watershed, and at each polygon the relative CN value was assigned. The simulated rain corresponds with the cumulative value calculated at 10 minutes interval (Fig. 3b). At the apex of each watershed a barrier of outflow points were

249 defined to obtain the total values of the watershed discharge. The simulation was performed
250 with a 20-m digital elevation model.

251

252 **3. Results**

253 During the Jova hurricane, lahars started in Montegrande ravine early in the morning of 12
254 October, 2011, around 07:20 GMT (here after all time is in GMT), after approximately 40
255 % of the total rain (240 mm) accumulated (Fig. 4a). The event lasted more than 4 hours,
256 and three main peaks in amplitude can be detected in the seismic signal (Fig. 4a). In
257 particular, the first two peaks are similar in amplitude (0.015 cm/s), separated by more than
258 2 hours of signal fluctuation. After less than one hour from the second peak, a single,
259 discrete pulse can be recognized (0.05 cm/s in amplitude), followed by a "train" of low-
260 amplitude seismic peaks that lasted for more than an hour.

261 Along the same ravine, an extreme event was recorded on 11 June, 2013. This event
262 corresponds to an extraordinary episode and is here introduced to better discuss the
263 hydrological response of the Montegrande ravine. It represents an unusual event at the
264 beginning of the rainy season, considering the total accumulated rainfall of 120 mm in less
265 than 3 hrs (Table 2), with maximum pick intensity up to 140 mm/hr (Fig. 4b). Based on the
266 seismic record and the still images of the event, this lahar was previously characterized as a
267 multi-pulse flow, with three main blocks-rich fronts (I, II and IV, Fig. 4c), with similar
268 amplitudes (0.015-0.025 cm/s), followed by a main flow body consisting of a homogenous
269 mixture of water and sediments (with a sediment concentration at the transition between a
270 debris flow and an hyperconcentrated flow) (III, Fig. 4c) (Vazquez et al. 2016a). The last,

271 more energetic pulse (0.042 cm/s) was accompanied by a water-rich frontal surge that was
272 able to reach the lens of the camera (IV, Fig. 4c). Comparing the Jova and the 2013 event
273 seismic records it is possible to note that in both events, the largest pulse corresponds with
274 the last one. Flow discharge was estimated for the 2013 event, with a maximum of 120 m^3/s
275 value for the largest pulse (IV, Figure 4b) (Vazquez et al., 2016a). For the Jova event, the
276 only visual data available are the images of the channel the day before and the day after the
277 event, where a deep erosion of the channel is visible (Fig. 5), but comparing its seismic
278 signal with the 2013 lahar, and based on the classification criterion established for lahars at
279 Volcán de Colima (Vazquez et al., 2016a) each main peak corresponds to the arrival of
280 flow surges or to block-rich fronts followed by the body of the flow. Fluctuation in seismic
281 energy along the vertical component reflects variation in flow discharge.

282 The lahar recorded during the Hurricane Manuel along the Montegrande ravine shows a
283 similar behavior as described for the Jova event (Fig. 6). As the event occurred during the
284 night no images are available. Based on the seismic record from the BB-RESCO, lahars
285 stated around 03:00, and lasted for seven hours. The event was characterized by five main
286 pulses, which amplitude increases with time (0.012-0.025 cm/s), being the last one the
287 larger in magnitude (0.04 cm/s). Based on the amplitude values, the first two peaks
288 correspond to precursory dilute flow waves followed by the three main pulses with block-
289 rich fronts (I, II and III, Fig 6).

290 For the Hurricane Patricia, seismic data (from the geophone) and still images were recorded
291 at the La Lumbre monitoring station. Based on these data, at approximately 21:22 a slurry
292 flow is detected on the main channel (Fig. 7a). First pulses of hyperconcentrated flows were
293 detected around 01:30 (24 October), which progressively increased in flow discharge and

sediment concentration. Several front waves were observed during flooding (I and II, Fig. 7b) for which an average flow discharge of 80-100 m^3/sec was estimated, and two main pulses arrived at 04:30 and 05:00, with 6 m-depth block-rich fronts and maximum flow discharge of 900 m^3/sec (III, IV, V and VI, Fig. 7b). At around 05:40 the seismic record detected the arrival of a third pulse. Although no images were available, the amplitude of the last pulse (0.07 cm/s) suggests it was larger than those previously described. As observed for the three events recorded at Montegrande ravine, the largest pulse corresponded again with the last one.

The results of rainfall simulations are plotted as a normalized curve of the total discharge, along with the normalized accumulated rainfall and its intensity (calculated over a 10-min interval) (Fig. 8). In the same plot, the arrival time of the main lahar pulses here analyzed is also indicated (red triangles, Fig. 8). By comparing watershed discharge with rainfall intensity, a general correlation can be observed for the Montegrande basin during Jova and Manuel hurricane, contrasting with the June 2013 event, where the simulation is not able to reproduce watershed discharge during the first minutes of the event when most of rainfall is accumulated and maximum rainfall intensities are detected. For la Lumbre watershed a clear correlation between peak intensities and watershed discharge is not clearly observable. If the arrival times of the main lahars' pulses are considered, the events associated to the hurricanes Jova and Manuel along the Montegrande ravine show a similar behavior. In both cases, early slurry flows are detected after ~40% of the total rain is accumulated. The main flow pulses better correlate with the highest rain intensity values, which also correspond with maximum peaks in watershed discharge; the last, largest pulse corresponds with the maximum peak discharge of the watershed. In contrast, for the

317 Patricia event, along the La Lumbre ravine, first slurry flows also starts after 40% or
318 rainfall accumulated, but main lahar pulses fit better with the peaks watershed discharge.
319 Finally, analyzing the simulation in the Montegrande ravine for the June 2013 event, it is
320 possible to observe a different behavior. The lahar starts as less than the 10% of rain is
321 accumulated, and the main lahar pulses perfectly correlate with the peak rainfall intensities,
322 and only the last largest pulse correlates with the watershed peak discharge.

323

324 **4. Discussion**

325 At present, several attempts to define lahar rainfall thresholds have been already carried out
326 for different volcanoes (i.e. Lavigne et al., 2000; van Westen and Daag, 2005 Barclay et al.,
327 2007), including Volcán de Colima (Capra et al., 2010). This study is mostly addressed to
328 better predict the lahar evolution during extraordinary hydrometeorological event as
329 hurricane, a common long-duration and large-scale rainfall phenomenon at tropical
330 latitudes. In particular, we are interested in predicting the arrival of block-rich fronts that
331 have caused several damages during past events. Based on the seismic and visual data
332 gathered from the events here analyzed, it is possible to evidence which are the key factors
333 in controlling the arrival of main lahars fronts. For Jova, Manuel and Patricia events, lahars
334 started after the 40% of total rain accumulated, and apparently the timing for the initial
335 pulses correlate well with the peaks of the rainfall intensity for the Montegrande ravine,
336 while for la Lumbre ravine they better match with the watershed discharge. Nevertheless
337 for all analyzed cases, the largest pulses correspond with the last ones and correlate with the
338 peak watershed discharge for all the analyzed examples. The observed difference between

339 Montegrande and La Lumbre ravines can be correlated with the different areas and shapes
340 of the two catchments. In fact, due to its elongated shape (K_G = 1.7) and small area (A = 2
341 km^2), the Montegrande watershed shows a quicker response between rainfall and discharge,
342 with a rapid water runoff that concentrated at different point along the main channel (Fig.
343 1b). This behavior is much clearer for the June 2013 event, which occurred at the beginning
344 of the rain season when soils on the lateral terraces of the ravines show a hydrophobic
345 behavior (Capra et al., 2010). The simulation is not able to reproduce any watershed
346 discharge at the beginning of the event, because the hydrophobic behavior of the soils
347 inhibits the infiltration and the water runoff quickly promotes lahar initiation. During this
348 event, the first lahar pulses perfectly match with the rainfall peak intensities (except for the
349 last major pulse), starting from the very beginning of the rainfall event. In contrast, La
350 Lumbre ravine has a wider, rounded upper watershed (K_G = 1.1; A = 14 km^2) that is able to
351 concentrated a larger volume of water before to turn SW in the main channel where lateral
352 contribution can still increase water discharge. Even if rainfalls of hurricanes Manuel and
353 Patricia show a similar behavior (Fig. 3), the catchment response of La Lumbre is clearly
354 different with a pulsating behavior of lahars mainly controlled by the watershed discharge.
355 Nevertheless, for all the events here analyzed, the largest pulse corresponds with the last
356 one recorded and it correlates with the maximum watershed discharge, pointing to a strong
357 control of the catchments recharge in generating the largest and more destructive pulses.
358 Previous works correlated the occurrence of surges within a lahar to multiple sources, such
359 as lateral tributaries along the main channel (i.e. Doyle et al., 2010) or due to the failure of
360 temporary dams of large clasts in correspondence of an increase in rainfall intensity (Kean
361 et al., 2013). Lateral tributaries are absent in both Montegrande and La Lumbre channels
362 and, even if accumulation of clasts it is possible, no significant discontinuities of the

channel bed can be observed upstream the monitoring sites. Based on data here presented, formation of pulses within a lahar is mostly controlled with the increase in water runoff that at a critical discharge rate mobilize a large volume of sediment where large clasts accumulate at its front. This is a well-documented mechanism (i.e. Iverson, 1997), but based on the model here proposed, the discharge rate is controlled by the watershed discharge that regulates the timing on the arrival of main pulses, depending on the rainfall behavior and the watershed shape. Nevertheless, the last pulse always is the largest in volume. This model is strictly related to migratory, long-duration and large-scale rainfall events hitting tropical volcanoes such as the Volcán de Colima. In fact, during mesoscale non-stationary rainfalls, typical at the beginning of the rainy season, lahars are usually triggered at low accumulated rainfall values and controlled by rainfall intensity due to the hydrophobic behavior of soils, and they usually consist of uni-pulse events with a single block-rich front that last less than one hour (i.e. Vázquez et al., 2016b). In perspective, the results here presented can be used to design an Early Warning System (EWS) for hurricane-induced lahars, i.e. event triggered by long-duration and large-scale rainfalls. Most common pre-event or advance-EWSs for debris flows are based on empirical correlations between rainfall and debris flow occurrence (e.g., Keefer et al., 1987; Aleotti, 2004; Baum and Godt, 2009). The instruments adopted for debris-flow advance warning are those normally used for hydrometeorological monitoring and consist of telemetry networks of rain gauges and/or weather radar. The typical way to represent these relations is identifying critical rainfall thresholds for debris flow occurrence. The availability of both a large catalogue of events and a reliable precipitation forecast that could give the predicted amount of rainfall some hours in advance would allow the issue of an effective warning, at least in predicting the arrival time of the main lahar pulses. In addition, instrumental

monitoring of in-channel processes can be used to validate a preliminary warning-condition triggered by ~~wheatear~~ weather forecast and/or rainfall measurements.

5. Conclusions

Real time monitoring of lahars at Volcán de Colima ~~volcanoes reveal~~ demonstrate that watershed discharge is the key factor in controlling the arrival of main block-rich fronts during long-lasting lahar triggered during tropical storms, and that the largest destructive pulses will arrive after the initial surging. For the 2015 Hurricane Patricia event the weather forecast predicted an estimated value for the total rainfall, ~~as~~ and also the approximate time of its landfall. Based on the ~~deigned~~ design storm obtained with the ~~time~~ rainfall/time distribution of the event here analyzed, it ~~could~~ would have been possible to anticipate when lahars started along the La Lumbre ravine, and the arrival time of main pulses. Along the other ravines, that show a watershed similar to the Montegrande, it ~~could~~ would have been possible to predict the arrival of at least the largest pulse. This information coupled with the real time monitoring could be a better tool for hazard assessment and risk mitigation. In fact, these findings can be used to implement an advance warning system based on the monitoring of a hydrometeorological process to issue a warning before a possible lahar is triggered.

Acknowledgements.

This work was supported by CONACyT projects 230 and 220786 granted to Lucia Capra and by the postdoctoral fellowship of DGAPA (Programa de Becas Posdoctorales de la

408 UNAM) granted to Velio Coviello. Thanks to José Luis Ortiz and Sergio Rodríguez, from
409 the Centro de Prevención de Desastres (CENAPRED), who set up the instrumentation on
410 the Montegrande monitoring site.

411

412 **References**

413 Aleotti P (2004) A warning system for rainfall-induced shallow failures. Eng. Geol. 73(3-
414 4): 247–265.

415 Barclay J, Alexander J, Susnik L (2007) Rainfall-induced lahars in the Belham valley,
416 Monserrat, West Indies. Journal of the Geological Society of London 164: 815-827.

417 Bartolini D, Borselli L (2009) Evaluation of the HydrologicSoil Group (HSG) with the
418 Procedure SCS Curve Number. In: Manualof Methods for Soil and Land Evaluation,
419 Edoardo A, Costantini C (ed), Science Publisher Inc., 600 pages. ISBN 978-1-57808-571-2

420 Baum R L, Godt JW (2009) Early warning of rainfall-induced shallow landslides and debris
421 flows in the USA. Landslides 7(3): 259–272.

422 Bendjoudi H, Hubert P (2002) Le coefficient de Gravélius : analyse critique d'un indice de
423 forme des bassins versants. J. Sci. Hydrol. 47: 921–930.

424 Capra L, Borselli L, Varley N, Norini G, Gavilanes-Ruiz JC Sarocchi D, Caballero L
425 (2010) Rainfall-triggered lahars at Volcán de Colima, Mexico: surface hydro-repellency as
426 initiation process. Journal of Volcanology and Geothermal Research 189(1-2): 105-117.

427 Cortes A, Macias JL, Capra L, Garduño-Monroy VH (2010) Sector collapse of the SW
428 flank of Volcán de Colima, México. The 3600 yr BP La Lumbre-Los Ganchos debris
429 avalanche and associated debris flows. Journal of Volcanology and Geothermal Research
430 197: 52-66.

431 Coviello V, Capra L, Vázquez R, Marquez-Hernández V, under revision. Seismic
432 characterization of hyperconcentrated flows in volcanic environment. Earth Surface
433 Processes and Landforms.

434 Cronin SJ, Hodgson KA, Neall VE, Palmer AS, Lecointre JA (1997) 1995 Ruapehu lahars
435 in relation to the late Holocene lahars of Whangaehu River, New Zealand. New Zealand
436 Journal of Geology and Geophisics 40: 507-520.

437 Davila N, Capra L, Gavilanes JC, Varley N, Norini G (2007) Recent lahars at Volcán de
438 Colima (Mexico): drainage variation and spectral classification. Journal of Volcanology
439 and Geothermal Research 165: 127-141.

440 de Bélizal E, Lavigne F, Hadmoko DS, Degai JP, Dipayana GA, Mutagin BW, Marfai MA,
441 Coquet M, Le Mauff B, Robin AK, Vidal C, Cholik N, Aisyah N (2013) Rain-triggered
442 lahars following the 2010 eruption of Merapi volcano, Indonesia: A major risk. Journal of
443 Volcanology and Geothermal Research 261: 330-347.

444 Doyle EE, Cronin SJ, Cole SE, Thouret JC (2010) The coalescence and organization of
445 lahars at Semeru volcano, Indonesia. Bulletin of Volcanology 72(8): 961-970.

446 Dumaisnil C, Thouret JC, Chambon G, Doyle EE, Cronin SJ (2010) Hydraulic, physical
447 and rheological characteristics of rain-triggered lahars at Semeru volcano, Indonesia. Earth
448 and Surface Processes and Landform 35: 1573-1590.

449 Ferrer-Julio M, Estrela T, Sanchez del Corral Jimenez A, Garcia-Melendez E (2003)
450 Generation of a curve number map with continuous values based on saturated hydraulic
451 conductivity. XI World Water Congress, 5-9 October 2003, Madrid, Spain: 1-10.
452 http://iwra.org/member/index.php?mainpage=&page=286&congressyear=2003

453 Gentile F, Bisantino T, Puglisi S, Trisorio Liuzzi G (2006) Analysis and modeling of debris
454 flows in Gargano watersheds (Puglia region, Southern Italy). WIT Transactions on Ecology
455 and the Environment 90: 181-191.

456 Hawkins RH, Hjelmfelt AT, Zevenbergen AW (1985) Runoff probability storm depth and
457 curve numbers. Journal of the Irrigation and Drainage Division 111: 330-340.

458 Kean W, McCoy S, Tucker G, Staley D, Coe J (2013) Runoff-generated debris flows:
459 Observations and modeling of surge initiation, magnitude, and frequency. Journal of
460 Geophysical Research: Earth Surface 118: 1-18.

461 Keefer DK, Wilson RC, Mark RK, Brabb EE, Brown WM, Ellen SD, Harp EL, Wieczorek,
462 GF, Alger CS, Zatkin RS (1987) Real-time landslide warning during heavy rainfall.
463 Science 238(4829): 921–5.

464 Iverson RM (1997) The physics of debris flows: Reviews of Geophysics 35: 245-296.

465 Lavigne F, Thouret JC, Voight B, Suwa H, Sumaryono A (2000) Lahars at Merapi volcano,
466 Central Java: an overview. Journal of Volcanology and Geothermal Research 100: 423-456.

467 Lavigne F, Thouret JC (2002) Sediment transport and deposition by rain-triggered lahars at
468 Merapi Volcano, Central Java, Indonesia. Geomophology 49: 45-69.

469 Llanes F, Ferrer PK, Gacusan R, Realino V, Obrique J, Eco RN, Lagmay AMF (2015)
470 Scenario-based maps using flo-2d and IFSAR-derived digital elevation models on the
471 November 2006 rainfall-induced lahars, Mayon Volcano, Philippines. ACRS 2015
472 Proceedings, Asian Association on Remote Sensing.

473 Marchi L, Arattano M, Deganutti A. (2002) Ten years of debris-flow monitoring in the
474 Moscardaro Torrent (Italian Alps), Geomorphology 46: 1–17, doi:10.1016/S0169-
475 555X(01)00162-3.

476 Mishra S K, Singh VP (2003) Soil conservation service curve number (SCS-CN)
477 methodology. Kluwer Academic Publishers, Dordrecht, Netherlands.

478 Natural Resource Conservation Services (2008) Rainfall-Frequency and Design Rainfall
479 Distribution for Selected Pacific Islands. Engineering Technical Note No. 3, United States
480 Department of Agriculture:115 pp.

not cited
481 O'Brien J, Julien P, Fullerton W (1993) Two-dimensional water flood and mudflow
482 simulation. J. Hydraul. Eng.-ASCE 119: 244-261.

483 Ortiz A. (2017) Modelado de conectividad y contribución de escorrentía superficial lateral
484 en la dinámica de flujos granulares de áreas volcánicas activas. PhD thesis, Universidad
485 Autónoma de San Luis Potosí, Facultad de Ciencias, México: 224 pp.

not cited.

Ortiz-Rodríguez AJ, Borselli L, Sarocchi D (2017) Flow connectivity in active volcanic areas: use of index of connectivity in the assessment of lateral flow contribution to main streams. Catena 157: 90 – 111.

Roverato M, Capra L, Sulpizio R, Norini G (2011) Stratigraphic reconstruction of two debris avalanche deposits at Colima Volcano (Mexico): Insights into pre-failure conditions and climate influence. Journal of Volcanology and Geothermal Research 207: 33-46.

Scott KM, Vallance JV, Kerle N, Macias JL, Strauch W, Devoli G (2005) Catastrophic precipitation-triggered lahars at Casita Volcano, Nicaragua: occurrence, bulking and transformation. Earth Surface Processes and Landforms 30: 59-79.

Sheridan MF, Connor CB, Connor L, Stinton AJ, Galacia O, Barrios G (2007) October 2005 Debris Flows at Panabaj, Guatemala: Hazard Assessment. American Geophysical Union, Spring Meeting 2007, abstract #V33A-07.

Takahashi T (2007) Debris Flow: Mechanics Prediction, and Countermeasures. Taylor and Francis/Balkema, Leiden: 448 pp.

Umbal JV, Rodolfo KS (1996) The 1991 lahars of southwestern Mount Pinatubo and evolution of the lahar-dammed Mapanuepe lake. Fire and mud; eruptions and lahars of Mount Pinatubo, Philippines, P. I. o. V. a. Seismology, ed., Quezon, Philippines: pp. 951-970.

USDA-NRCS (U.S. Department of Agriculture-Natural Resources Conservation Service). (2007) Hydrologic soil groups. National engineering handbook. Part 630 hydrology, Washington, DC.

van Westen CJ, Daag AS (2005) Analysing the relation between rainfall characteristics and lahar activity at Mount Pinatubo, Philippines. Earth and Surface Processes and Landform 30: 1663-1674.

Van Wyk Vries B, Kerle N, Petley D (2000) Sector collapse forming at Casita volcano, Nicaragua. Geology 28(2): 167-170.

Vázquez R, Suriñach E, Capra L, Arámbula-Mendoza R, Reyes-Dávila G (2016a) Seismic characterisation of lahars at Volcán de Colima, Mexico. Bulletin of Volcanology 78: 8.

Vázquez R, Capra L, Coviello V (2016b) Factors controlling erosion/deposition phenomena related to lahars at Volcán de Colima, Mexico. Natural Hazards and Earth System Sciences 16: 1881–1895.

Zanuttigh B, Lamberti A (2007) Instability and surge development in debris flows. Rev. Geophys. 45: RG3006, doi:10.1029/2005RG000175.

Zobin VM, Placencia I, Reyes G, Navarro C (2009) The characteristics of seismic signal produced by lahars and pyroclastic flows: Volcán de Colima, Mexico. Journal of Volcanology and Geothermal Research 179: 157-167.

Figure captions

Figure 1. a) Aster image (4, 5 and 7 bands in RGB combination) where main watersheds at Volcán de Colima are represented. The locations of the monitoring stations are indicated. The inset show the location of the raingauge of the Meteorological National Service at the summit of the Nevado de Colima Volcano.

Figure 2. a) Panoramic view of the Volcán de Colima showing the unvegetated main cone mostly composed by loose volcanic fragments. b) Montegrande and c) La Lumbre ravines in the middle reach where it is possible to observe the main channel flanked by 10-15m high terraces mainly constituted by debris avalanche deposits.

Figure 3. a) Cumulative and b) normalized values of rainfall of hurricanes Jova, Manuel and Patricia calculated at 10 min-intervals. c) Normalized curve of total rainfalls cumulated at 15, 30, 60 minutes and 1, 3, 6, 12, 18, 24, 28 hrs. Dotted line represents the average value between Manuel and Patricia hurricanes.

Figure 4. a) Seismic record of the lahar triggered during the Hurricane Jova, on 12 October, 2011. b) Seismic record of the lahar triggered during the 11 June, 2013 events. Main pulses are indicated with roman letters. c) Images captures by the camera corresponding to the main lahar pulses as indicated in figure b.

Figure 5. Images showing the morphology of the channel at the monitoring site of the Montegrande ravine, a) the day before and b) the day after the Hurricane Jova. c) Topographic profiles showing that the channel was eroded 1.5 m in depth.

543 Figure 6. Seismic record of the lahar triggered during the Hurricane Manuel, on 15
544 September, 2013, recorded along the Montegrande ravine

545 Figure 7. a) Seismic record of the lahar triggered during the Hurricane Patricia, on 26
546 October, 2015, recorded along the La Lumbre ravine. Main lahar pulses are indicated with
547 roman letters. b) Images captured by the camera corresponding to the main pulses as
548 indicated in figure a.

549 Figure 8. Diagrams showing the main lahar pulses (red triangles) as detected from the
550 seismic signal of the analyzed events in relation with the accumulated rainfall (dark line),
551 rainfall intensity (10m/hr) (gray line) and simulated watershed discharge (blue line) for the
552 following hidrometeorological events a) Jova; b) Manuel; c) 13 June, 2013; and d) Patricia.

553 Table 1. Data collected for the events here studied.
554

555 Table 2. Normalized accumulated rains (in percentage) at progressive time steps.

556

Table 1. Data collected for the events here studied.

Event	ravine	Seismic record	Image record	Total rain (mm)	Max. rain intensity (mm/hr)
Jova	Montegrande			240	43
Manuel	Montegrande	X		300	32
Patricia	Lumbre	X	X	400	37
11 June 2013	Montegrande	X	X	120	140

Add dates...

28 in text

Table 2. Normalized accumulated rains (in percentage) at progressive time steps.

Event/time (hrs)	0.25	0.5	1	2	3	6	12	24	27
Jova	0.0011	0.0016	0.0035	0.0172	0.0329	0.1411	0.7073	0.968	0.9943
Manuel	0.0023	0.0035	0.0042	0.0072	0.0151	0.0341	0.1548	0.735	0.9181
Patricia	0.0002	0.0004	0.0009	0.0062	0.0174	0.0556	0.2544	0.829	0.9782
average	***0.00125***	***0.00195***	***0.00255***	***0.0067***	***0.01625***	***0.04485***	***0.2046***	***0.782***	***0.9481***

The average values refer to hurricanes Manuel and Patricia.

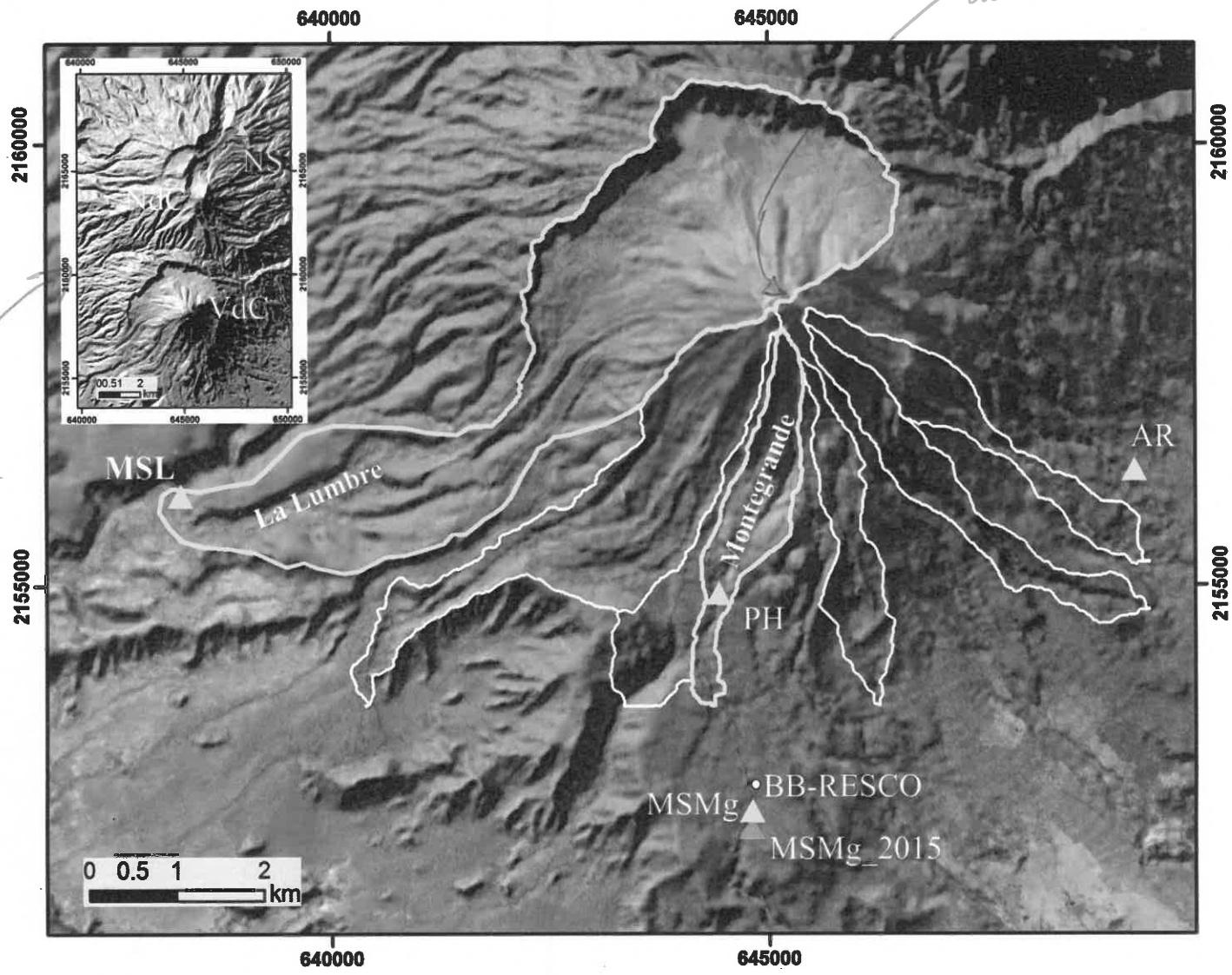

altitude in m ASL?

reduce inset with location of VdC in Mexico

OK, so rain gauge is 10km away & on another mountain...

Figure 01

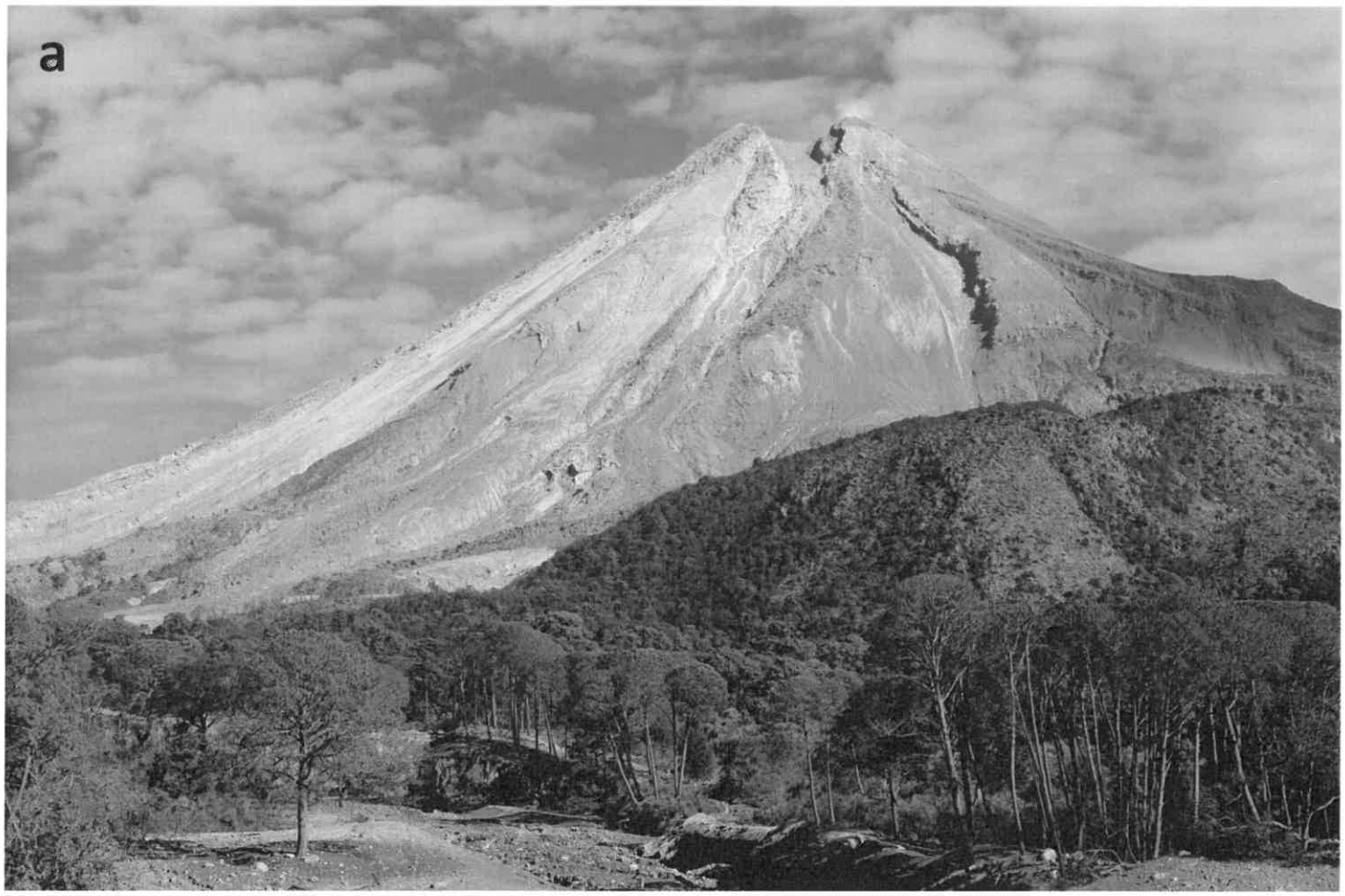

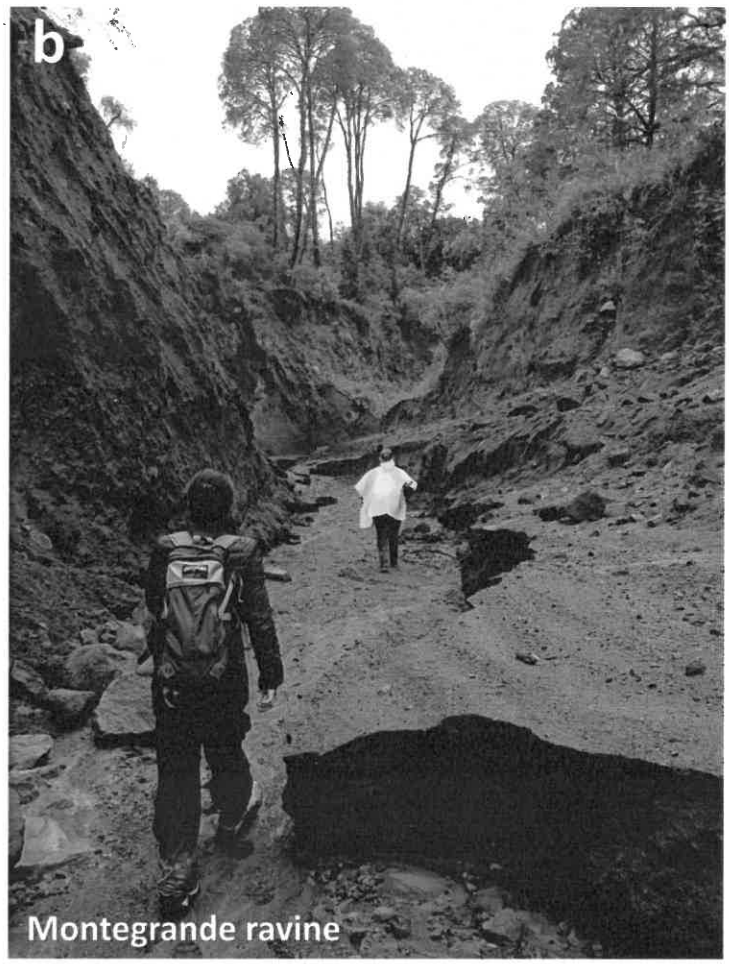

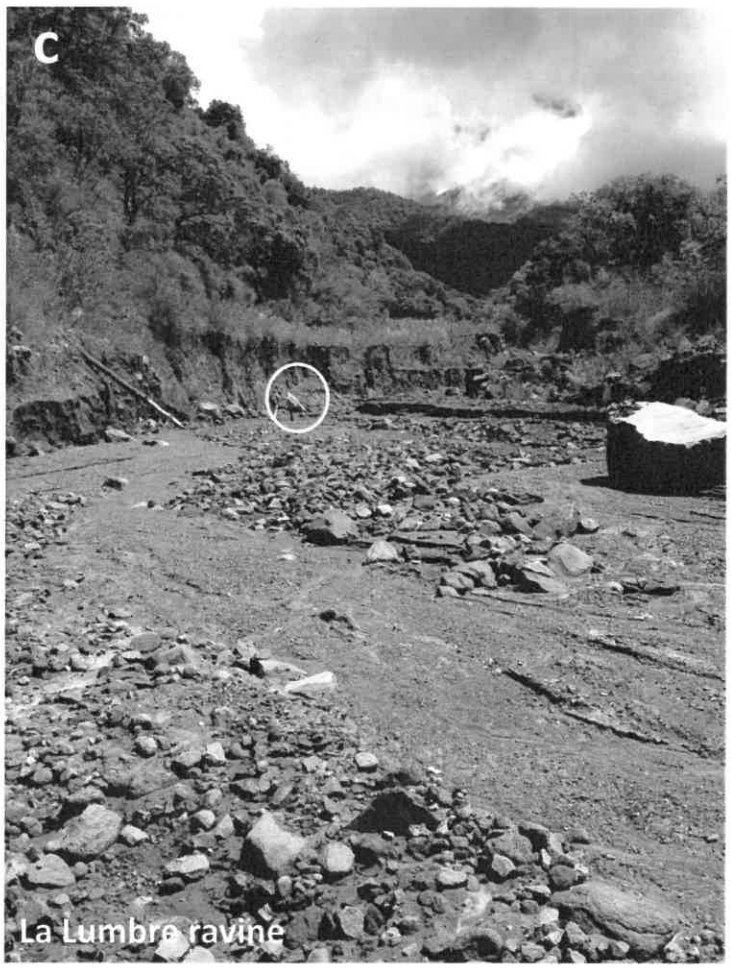

Figure 02

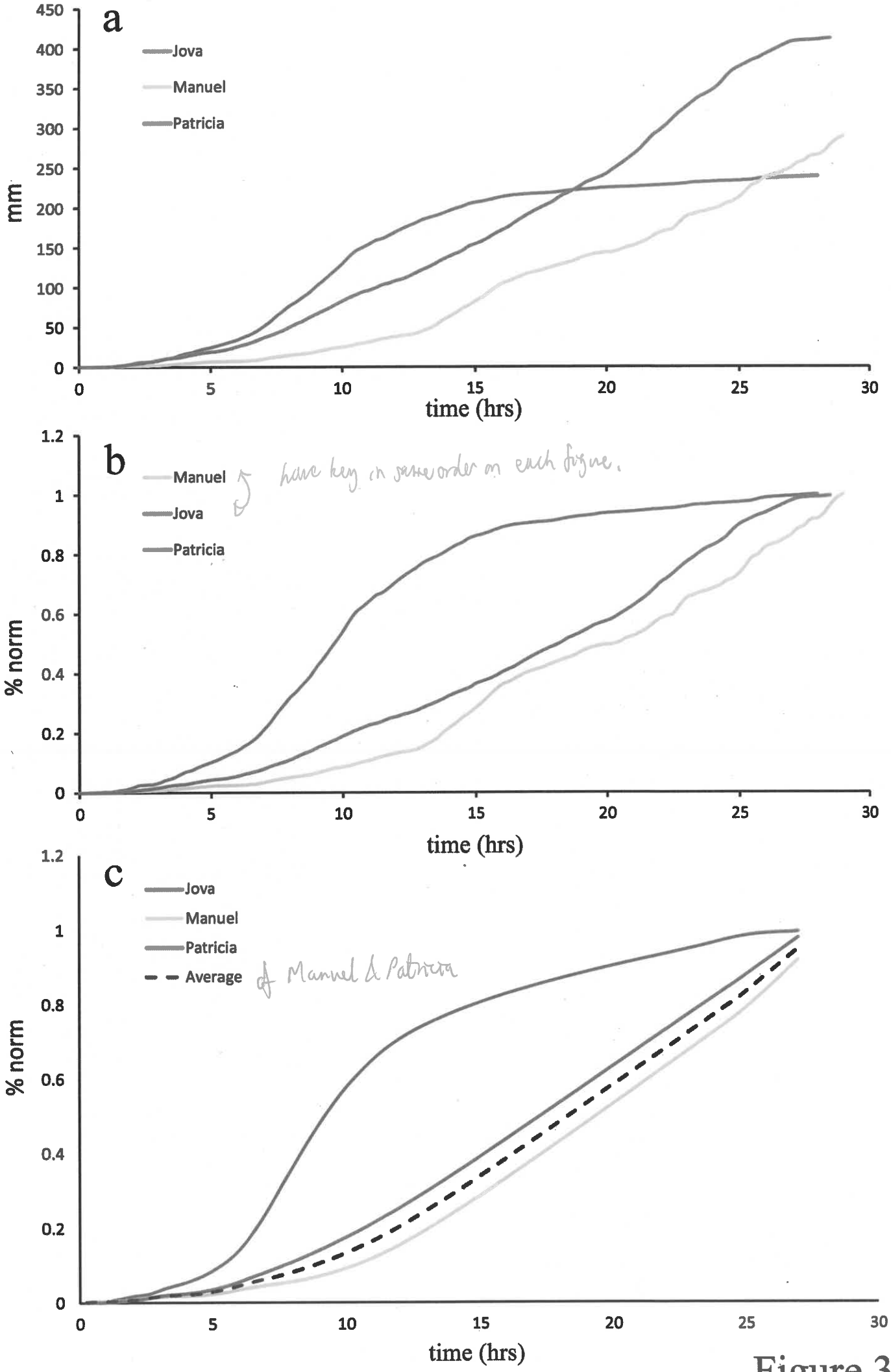
a
Jova
Manuel
Patricia
mm
time (hrs)
b
Manuel
Jova
Patricia
have key in same order on each figure.
% norm
time (hrs)
c
Jova
Manuel
Patricia
Average
of Manuel & Patricia
% norm
time (hrs)

Figure 3

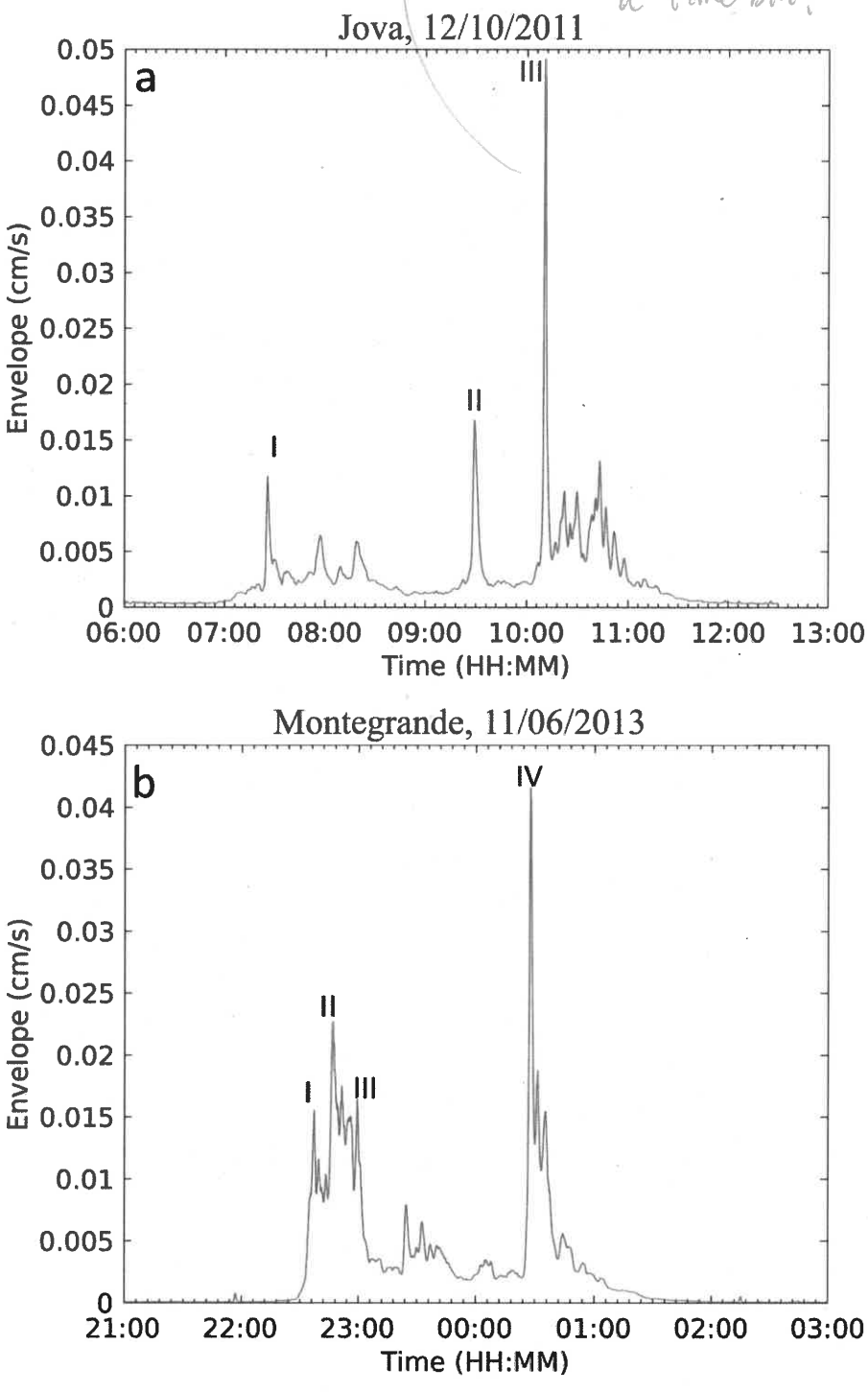
Jova, 12/10/2011
a
I
II
III
Envelope (cm/s)
0.05
0.045
0.04
0.035
0.03
0.025
0.02
0.015
0.01
0.005
0
06:00
07:00
08:00
09:00
10:00
11:00
12:00
13:00
Time (HH:MM)
Montegrande, 11/06/2013
b
I
II
III
IV
Envelope (cm/s)
0.045
0.04
0.035
0.03
0.025
0.02
0.015
0.01
0.005
0
21:00
22:00
23:00
00:00
01:00
02:00
03:00
Time (HH:MM)

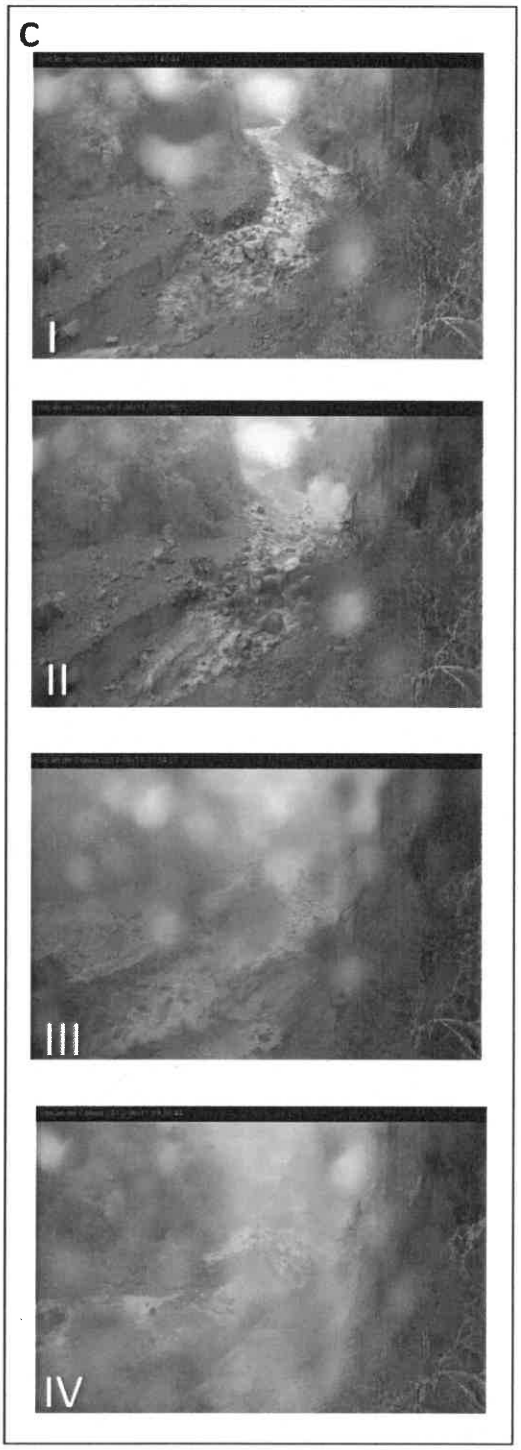
c
I
II
III
IV

Figure 4


a
2 m
11 Oct, 2011


b
3.2 m
12 Oct, 2011

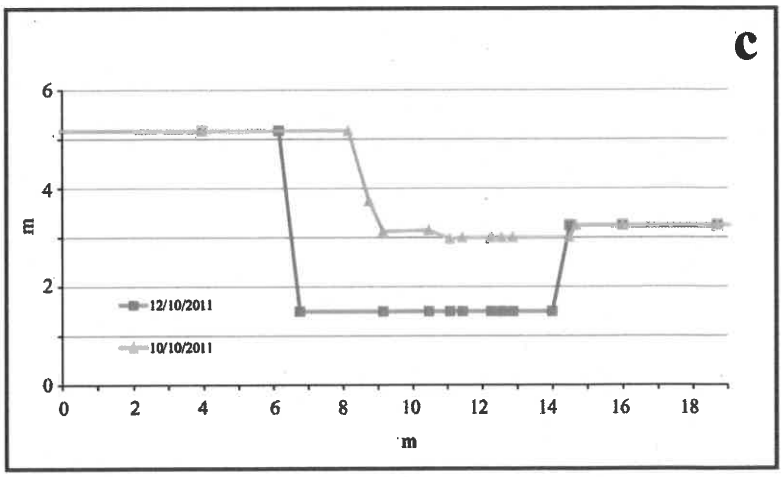
c
6
4
2
0
m
0
2
4
6
8
10
12
14
16
18
m
12/10/2011
10/10/2011

Figure 5

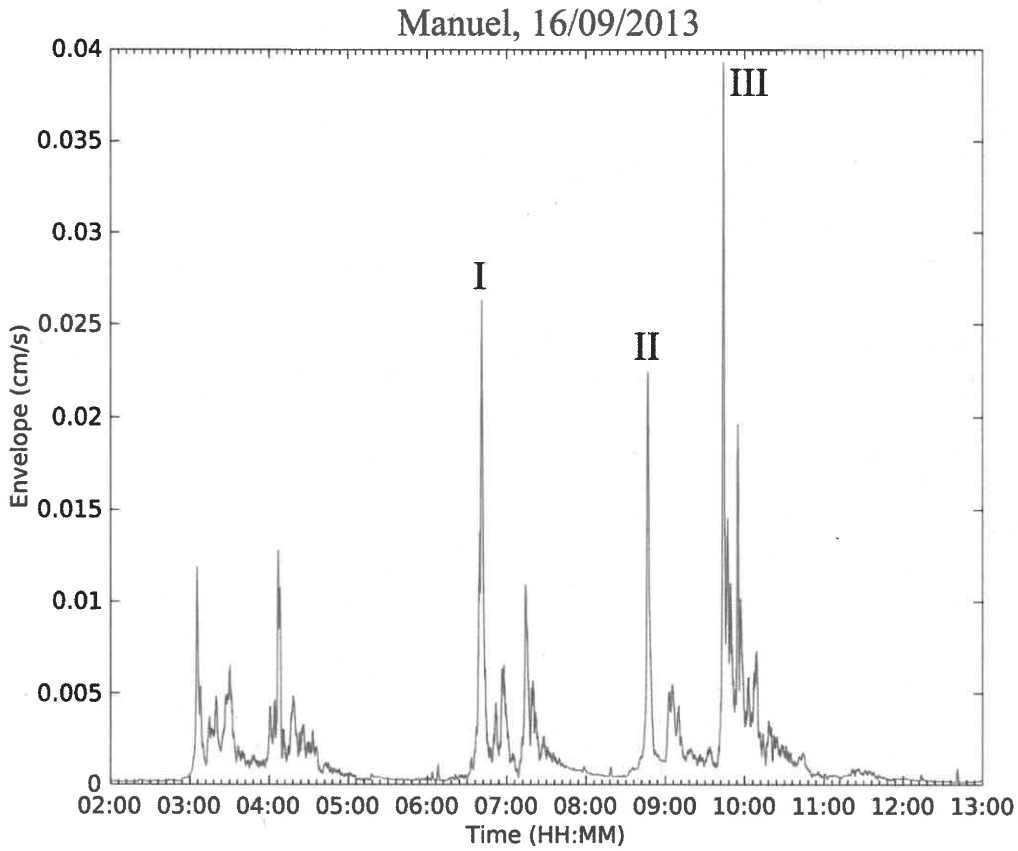
Manuel, 16/09/2013
0.04
0.035
0.03
0.025
0.02
0.015
0.01
0.005
0
Envelope (cm/s)
I
II
III
02:00
03:00
04:00
05:00
06:00
07:00
08:00
09:00
10:00
11:00
12:00
13:00
Time (HH:MM)

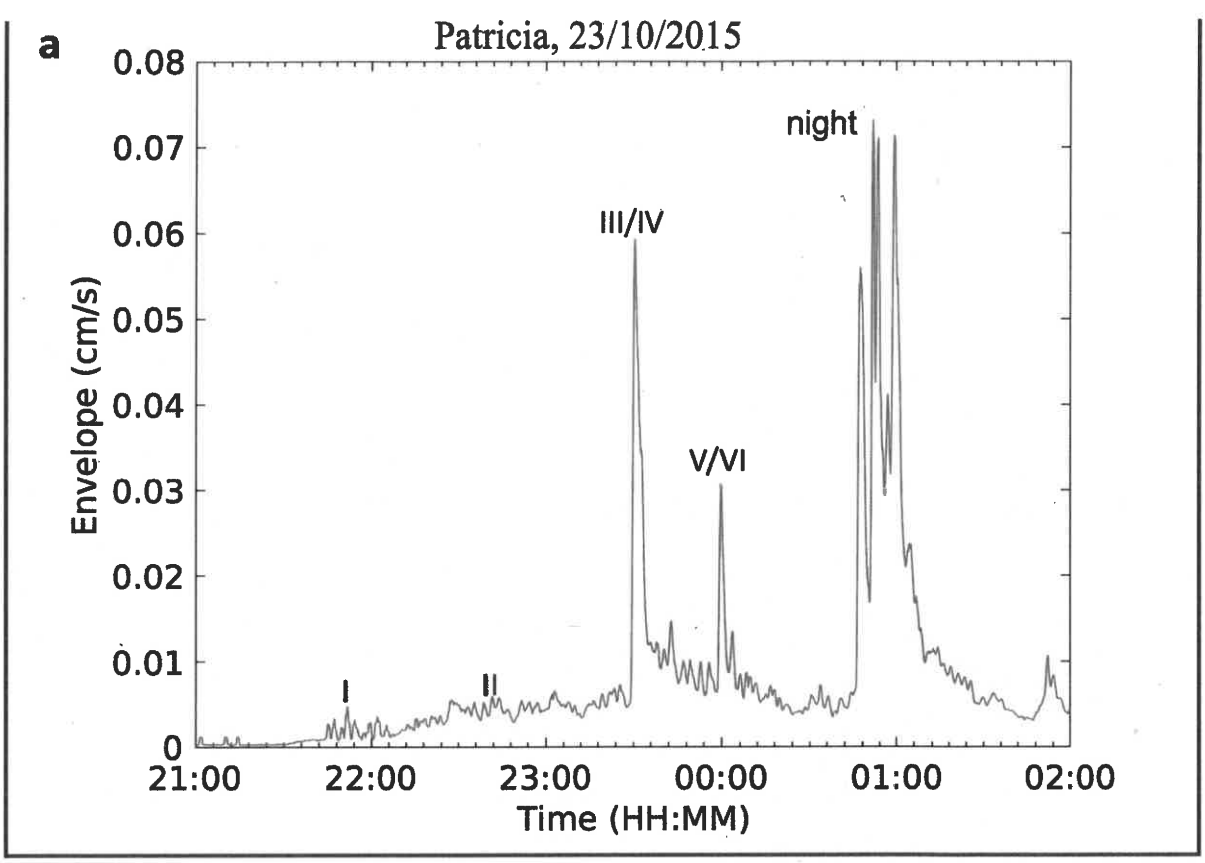
a
Patricia, 23/10/2015
Envelope (cm/s)
0.08
0.07
0.06
0.05
0.04
0.03
0.02
0.01
0
night
III/IV
V/VI
I
II
21:00
22:00
23:00
00:00
01:00
02:00
Time (HH:MM)

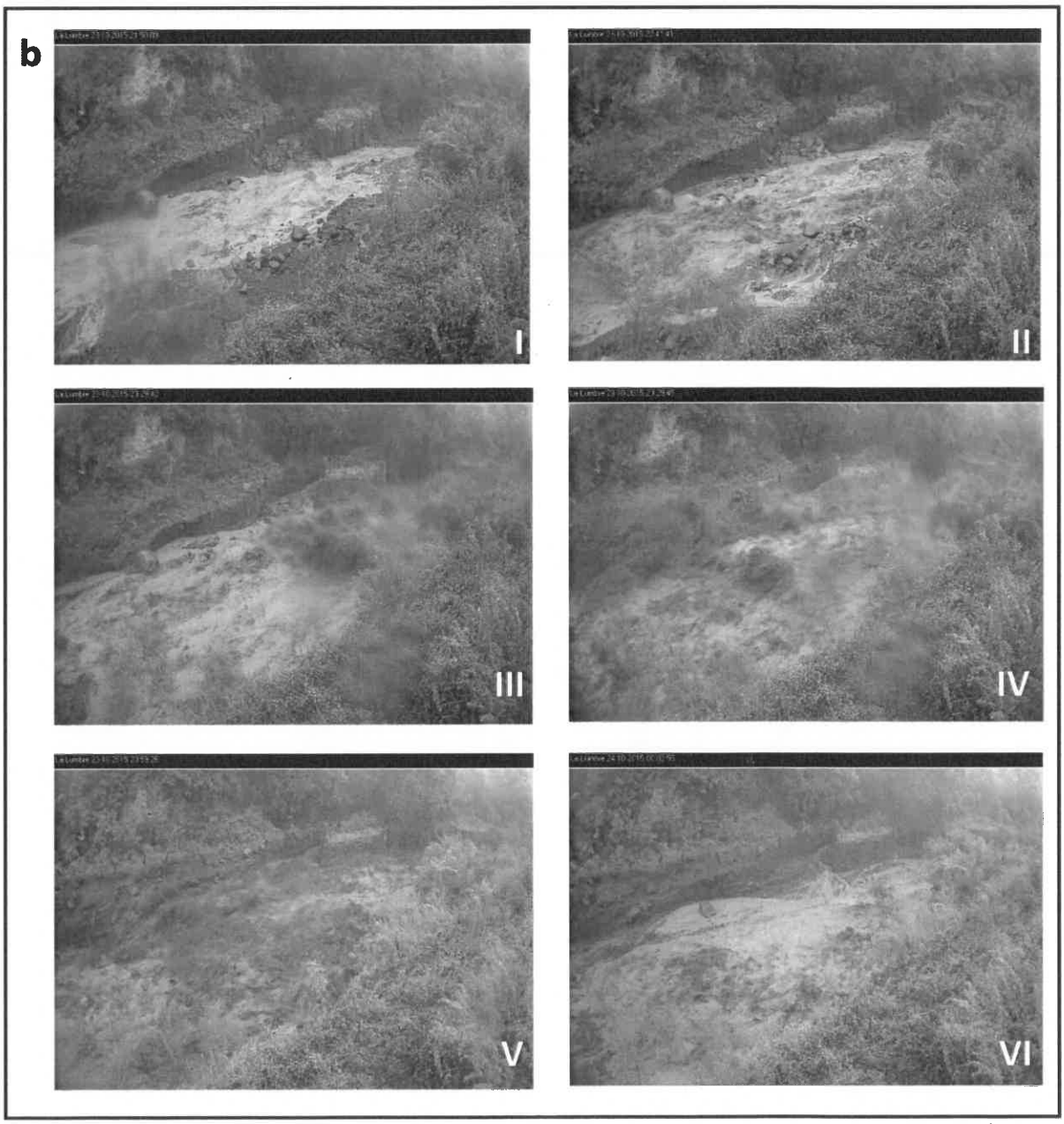
b
I
II
III
IV
V
VI

Figure 7

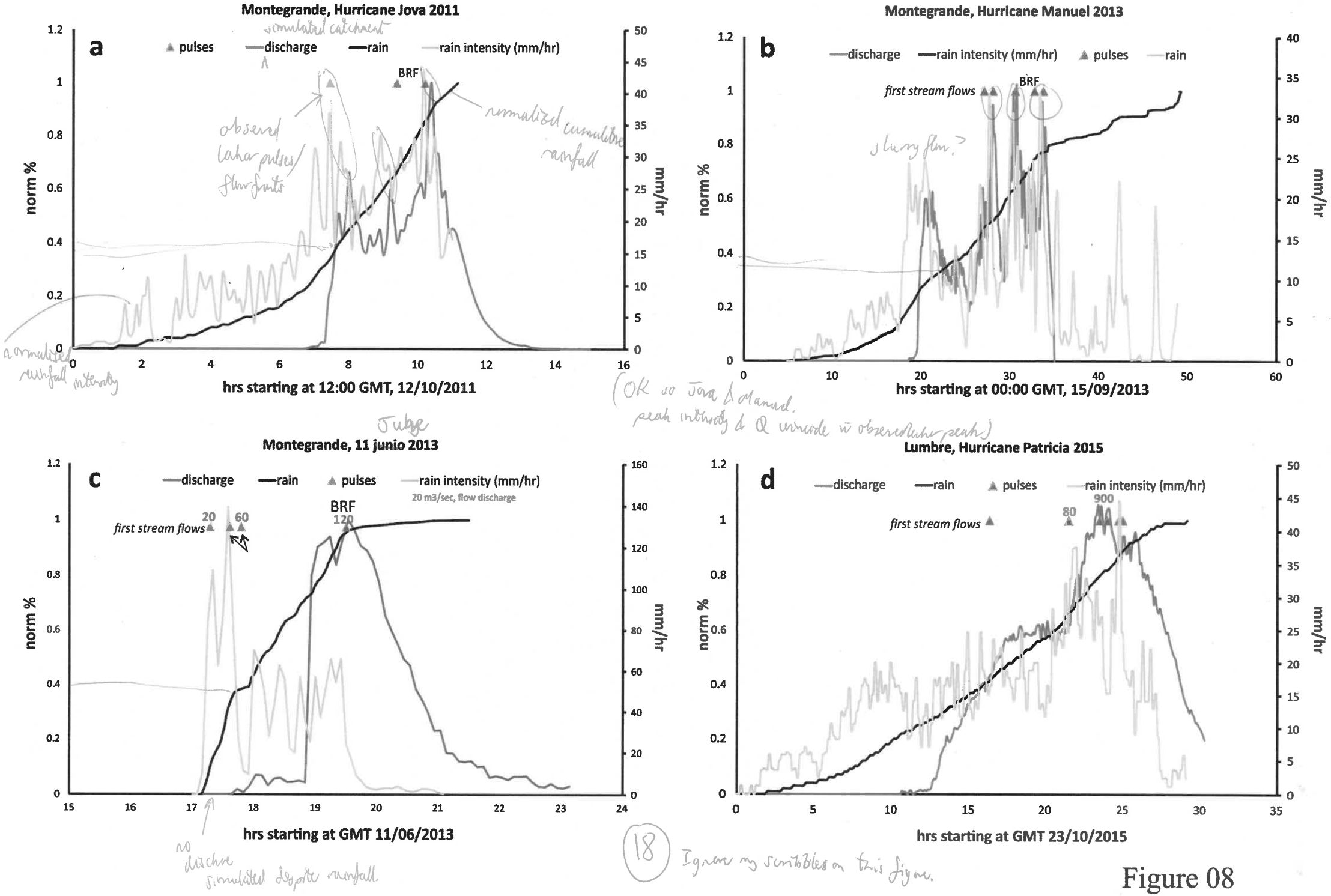
Montegrande, Hurricane Jova 2011
a
pulses
discharge
rain
rain intensity (mm/hr)
BRF
norm %
mm/hr
hrs starting at 12:00 GMT, 12/10/2011
Montegrande, Hurricane Manuel 2013
b
discharge
rain intensity (mm/hr)
pulses
rain
first stream flows
BRF
norm %
mm/hr
hrs starting at 00:00 GMT, 15/09/2013
Montegrande, 11 junio 2013
c
discharge
rain
pulses
rain intensity (mm/hr)
20 m3/sec, flow discharge
first stream flows
20
60
BRF
120
norm %
mm/hr
hrs starting at GMT 11/06/2013
Lumbre, Hurricane Patricia 2015
d
discharge
rain
pulses
rain intensity (mm/hr)
first stream flows
80
900
norm %
mm/hr
hrs starting at GMT 23/10/2015

Figure 08